Chaos ARTICLE scitation.org/journal/cha

Multifractal structure of the monthly rainfall regime in Catalonia (NE Spain): Evaluation of the non-linear structural complexity

Cite as: Chaos **30**, 000000 (2020); doi: 10.1063/5.0010342
Submitted: 10 April 2020 · Accepted: 16 June 2020 ·
Published Online: [redacted] 2020

View Online Export Citation CrossMark

X. Lana,[a] R. Rodríguez-Solà, M. D. Martínez, M. C. Casas-Castillo, C. Serra, and R. Kirchner

AFFILIATIONS

Department of Physics, Polytechnic University of Catalonia, UPC 1-3, Jordi Girona Street, 08034 Barcelona, Spain

[a]**Author to whom correspondence should be addressed:** francisco.javier.lana@upc.edu

ABSTRACT

The complex non-linear regime of the monthly rainfall in Catalonia (NE Spain) is analyzed by means of the reconstruction fractal theorem and the multifractal detrended fluctuation analysis algorithm. Areas with a notable degree of complex physical mechanisms are detected by using the concepts of persistence (Hurst exponent), complexity (embedding dimension), predictive uncertainty (Lyapunov exponents), loss of memory of the mechanism (Kolmogorov exponent), and the set of multifractal parameters (Hölder exponents, spectral asymmetry, spectral width, and complexity index). Besides these analyses permitting a detailed description of monthly rainfall pattern characteristics, the obtained results should also be relevant for new research studies concerning monthly amounts forecasting at a monthly scale. On one hand, the number of necessary monthly data for autoregressive processes could change with the complexity of the multifractal structure of the monthly rainfall regime. On the other hand, the discrepancies between real monthly amounts and those generated by some autoregressive algorithms could be related to some parameters of the reconstruction fractal theorem, such as the Lyapunov and Kolmogorov exponents.

The monthly rainfall regime in Catalonia, NE Spain, is analyzed by means of the fractal theory with the aim of improving the knowledge about its complex physical mechanism.

I. INTRODUCTION

The fractal structure of nature phenomena can be successfully analyzed by taking Mandelbrot (1983) as a reference. More concretely, the physical mechanisms of these phenomena can be studied by taking into account concepts such as predictive instability, degree of complexity, and loss of memory of the physical mechanism (Turcotte, 1997; Diks, 1999; and Dimr, 2005). Another relevant point of view is the analyses of these phenomena by means of the multifractal theory (Goltz, 1997) and, more concretely, by means of specific algorithms applied to time series (Kantelhardt *et al.*, 2002). Some examples of these fractal and multifractal analyses on solid Earth sciences (seismology and tectonics) are Hirabayashi *et al.* (1992), Godano *et al.* (1996), Enescu *et al.* (2005), and Ozturk (2012), among others. With respect to dynamic atmospheric and climatology, Koscienly-Bunde *et al.* (1998), Talkner and Weber (2000), García-Marín *et al.* (2013; 2019), Rodríguez *et al.* (2013), Burgueño *et al.* (2014), Lana *et al.* (2015; 2016), and Herrera-Grimaldi *et al.* (2019) , among others, can be cited.

By focusing the analysis on the characteristics of a rainfall regime, a detailed analysis of its complexity could permit a better detection of regions where rainfall amount forecasting is quite easy or, alternatively, difficult, and of high uncertainty. The complexity of a rainfall regime could be quantitatively evaluated by fractal and multifractal theories. The application of the reconstruction fractal theorem (RFT) (Diks, 1999) to monthly amount series permits one to quantify several concepts such as persistence or randomness of the time series (Hurst exponent), predictive uncertainty (Lyapunov exponents), complexity of the physical process (embedding dimension), and loss of memory of the physical system (Kolmogorov entropy). The multifractal behavior, determined by the multifractal detrended analysis (MDFA) (Kantelhardt *et al.*, 2002), quantifies the complexity of the physical mechanism bearing in mind the central, maximum, and minimum Hölder exponents; spectral amplitude and asymmetry; as well as a complexity index that summarizes these multifractal parameters.

The main objective of this study is a detailed analysis of the spatial distribution of fractal and multifractal parameters characterizing the complexity of the monthly pluviometric regime of a Mediterranean area, Catalonia, where a homogeneous *Mediterranean climate* is not expected due to its varied and complex topography. As a consequence, advantages and shortcomings concerning monthly amounts forecasting and possible time trends on monthly amounts could be relevant. On one hand, different levels of the monthly regime complexity could be detected for the different climatic areas of Catalonia. On the other hand, monthly rainfall forecasting uncertainties could be expected with a certain degree of veracity. The randomness or persistence of the monthly pluviometric series is quantified by the Hurst exponent. The complexity of the physical process governing the pluviometry of the different climatic areas is characterized by the embedding dimension concept (number of non-linear equations to describe the physical mechanism), and the uncertainty degree on forecasting monthly amounts is assumed to be strongly related to the Lyapunov exponents. Additionally, the Kolmogorv entropy permits quantification of the loss of memory of the physical mechanism, this question being a relevant factor if autoregressive processes are applied to forecast monthly rainfall amounts. The complexity of the rainfall regime is described from different points of view based on the multifractal spectrum (maximum, minimum, and central Hölder exponents; spectral amplitude; and spectral asymmetry) all of them being summarized by a complexity index. The results obtained in these fractal and multifractal analyses permit a detailed description, at a local scale, of the physical mechanisms complexity governing the pluviometry of an area of varied topography. In short, improvements on monthly rainfall forecasting and validation of monthly amount time trends should be expected.

The contents of this paper are organized as follows. The quality of the dataset and the recording continuity are discussed in Sec. II. The RFT theorem and the MDFA algorithm are described with detail, being also explained the meaning of the corresponding fractals parameters in terms of monthly rainfall regimes, in Sec. III. The obtained results are introduced in detail in Sec. IV and the relevance of them, with possible improvements on rainfall forecasting at a monthly scale and verification of possible time trends on monthly amounts, are summarized in Sec. V.

II. STUDY AREA AND DATABASE

The area of the Iberian Peninsula corresponding to Catalonia (NE Spain) should be identified as belonging to a Mediterranean climate in agreement with the Köppen–Geiger classification (Mc Night and Hess, 2000), bearing in mind its latitude on the Northern Hemisphere and the characteristics of several climatic variables. Nevertheless, some relevant differences on thermometric and pluviometric regimes within the territory have to be taken into consideration due to the relatively complex orography (Fig. 1) and the temperate effects of the Mediterranean Sea on areas close to the Mediterranean coast, whereas the littoral fringe is characterized by moderate low temperatures in winter and notable hot episodes in summer, the inner areas, delimited by the Pre-Littoral chains, the Eastern Pyrenees, and the Ebro valley, are characterized by cold winters and very hot summers. Annual average temperatures vary from 0°C (Pyrenees) to 17 °C (inner areas), and the extreme temperature records are within a very wide range of 75 ° (maximum 43 °C for inner Catalonia and minimum −32 ° for the Pyrenees). With respect to the pluviometric regime, the complex topography also contributes to different spatial distributions of rainfall amounts, and three different domains could be assumed, whereas Pyrenees and Pre-Pyrenees areas are characterized by average annual amounts close to or exceeding 1000 mm/yr, sometimes with copious snow episodes (especially for the north face of the Pyrenees), some places of the Pre-Littoral chain achieve amounts close to or slightly exceeding 700 mm/yr, and the records of the rest of territory (inner Catalonia and Littoral fringe) range from 300 to 700 mm/yr. Consequently, the expected equinoctial thermometric and rainfall regimes are only explicitly accomplished in the Littoral fringe and some inner domains, being a relevant factor for the rest of the territory the Pre-Littoral and Eastern Pyrenees chains. In short, bearing in mind rainfall temperatures and wind regimes, five different climate domains, all of them within a generic *Mediterranean climate*, can be established for Catalonia. These five domains would be that corresponding to Littoral fringe, Inner territory, Mediterranean-mountain, transition from Mediterranean to Atlantic domain, and Atlantic Mountain (the last one a small domain in the north face of the Pyrenees). Previous recent analyses of pluviometry and thermometric regimes in Catalonia can be found in Burgueño *et al.* (2014), Lana *et al.* (2016), and Casas-Castillo *et al.* (2018), among others, who have recently analyzed them at local and regional scales. A very detailed description of thermometric and pluviometric regimes can be also found in Clavero *et al.* (1996).

Due to the relative complex orography of Catalonia (Fig. 1), with altitudes about sea level achieving 2900 m in the Pyrenees,

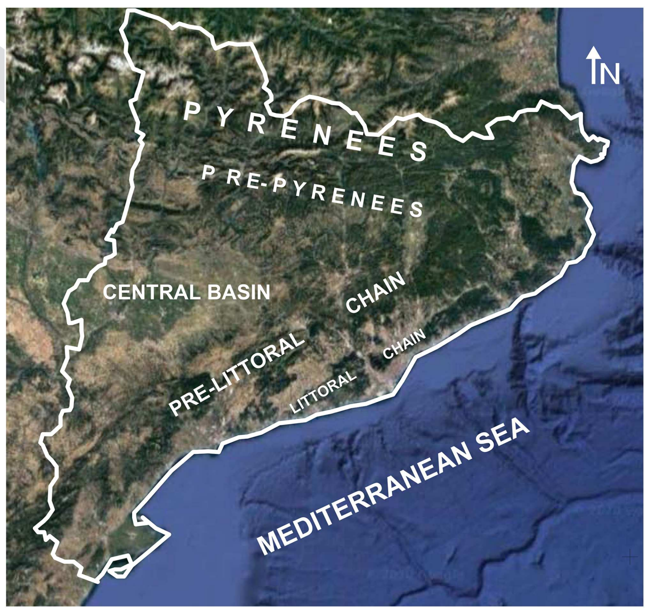

FIG. 1. Topographic image with the most relevant orographic elements (Eastern Pyrenees, Central Basin, and Littoral and Pre-Littoral chains).

2000 m on the Pre-Pyrenees, varying from 900 to 1500 m in the Pre-Littoral chain, close to 500–600 m in the Central Basin, and only a few hundred meters on the Littoral chain, a pluviometric network as dense as possible is necessary. Monthly rainfall amount series have been collected from Servei Meteorològic de Catalunya (SMC, www.meteo.cat), the meteorological agency of Catalonia, including records of two other organisms: Fabra Observatory (Reial Acadèmia de Ciències i Arts, RACA, Barcelona) and Ebre Observatory (Ramon Llull University, URL, and CSIC, Consejo Superior de Investigaciones Científicas, CSIC, Spanish Government). A set of 96 monthly amount series [Fig. 2(a)] have been selected, offering the emplacement of the rain gauges a relatively dense spatial distribution and, at the same time, accomplishing relevant conditions. First, several tests of homogeneity and data quality were applied at daily scale by Llabrés-Brustenga *et al.* (2019) to distinguish the acceptable rainfall series. Second, for very short lags of few days without records, unknown daily rain amounts have been substituted by those generated by a kriging process (Stein, 1999 and Press *et al.*, 2007), taking into account daily records close to the gauge without data and the topography of the area including these emplacements have been taken in this kriging process. Third, an appropriate length (40 years interval) for a right computation of fractal parameters has been considered. The results of applying these constraints are illustrated in Fig. 2(b), where the chosen 96 rainfall records represent 80%–100% of the available data for 1960–2000.

A first description of the rainfall regime is shown in Figs. 3(a) and 3(b), where the spatial distribution of the average annual rain amounts and the standard deviations are represented. The differences on the average amounts at annual scale are quite evident by comparing Littoral and Pre-Littoral emplacements (500–800 mm/yr), areas of the Central basin (300–500 mm/yr), as well as emplacements close to the Eastern Pyrenees and the Pyrenees chain itself (800–1000 mm/yr and 1100 mm/yr in a few places). It is also remarkable the high standard deviations for many areas, including the Pyrenees area, being this fact in agreement with the expected irregularity of a Mediterranean rainfall regime. In fact, the spatial patterns of the geographical distribution of average and standard deviation are quite similar, with a quite evident tendency to increase the standard deviations with the average amounts.

III. FRACTAL AND MULTIFRACTAL THEORY

A. Reconstruction theorem

1. Rescaled-range analysis

A first step on a fractal analysis of time series could be the process designed as the rescaled-range analysis (Korvin, 1992), which is quantified by the power law,

$$\frac{R(\tau)}{S(\tau)} \propto \tau^{H}, \tag{1}$$

with $R(\tau)$ and $S(\tau)$ being the range of variation and standard deviation, respectively, of segments of length τ and H, the Hurst exponent of Eq. (1). If this power-law equation is well accomplished, the time series could be qualified as random (H very close to 0.5), persistent (H notably exceeding 0.5), or anti-persistent (H clearly lowering 0.5). Besides a possible way of self-similar/affine character verification of the series (Turcotte, 1997), the numeric values of H permit to decide if the randomness of the series discourages forecasting strategies or the persistent/anti-persistent character facilitates successful application of forecasting algorithms.

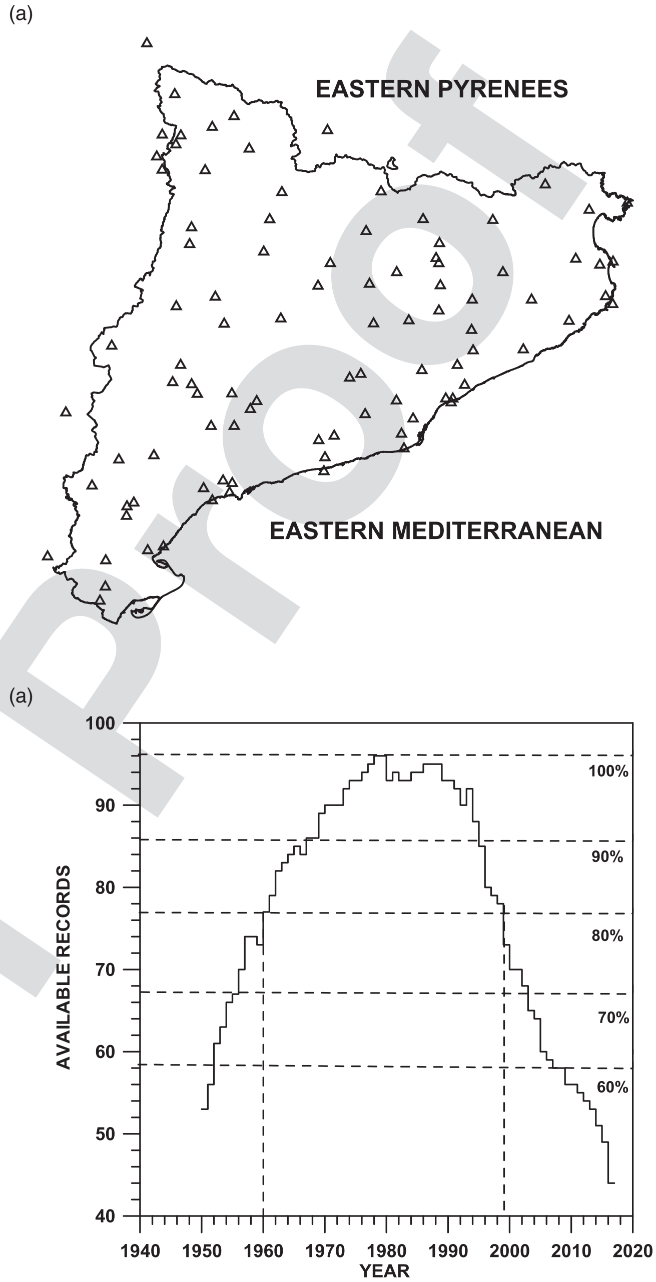

FIG. 2. (a) Pluviometric network with the location of the 96 rain gauges (open triangles). (b) Annual evolution of the number of available gauges. Vertical dashed lines limit the chosen 40 years interval for the analysis.

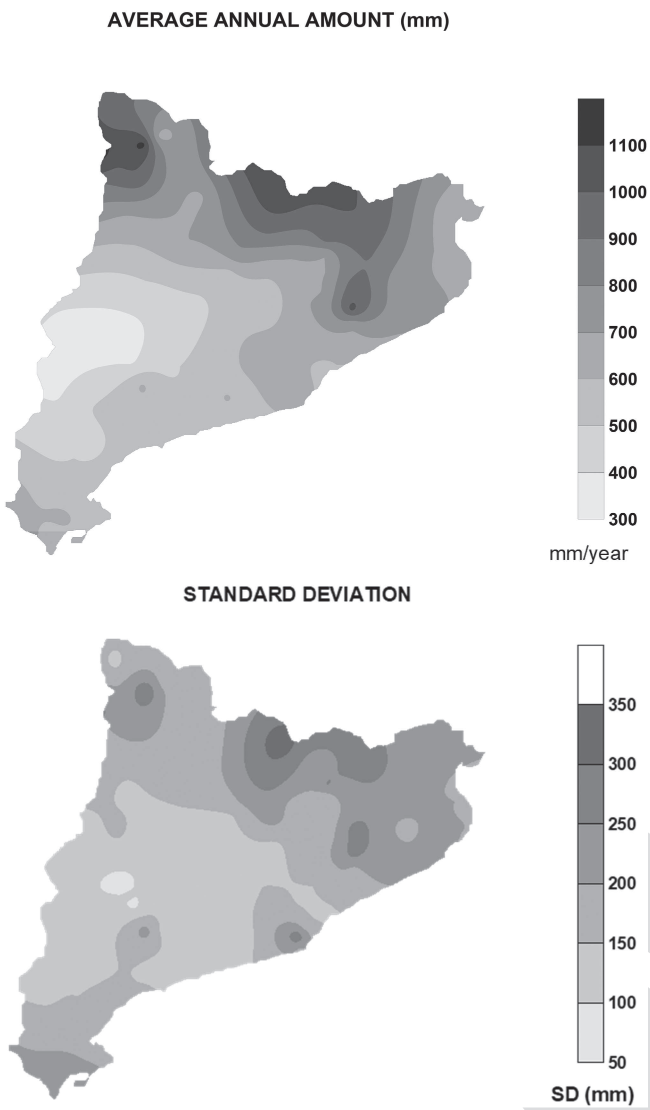

FIG. 3. Spatial distribution of the average annual rainfall amounts and their standard deviations.

2. Reconstruction fractal theorem

The reconstruction theorem (Diks, 1999) permits one to quantify the complexity and predictive instability of a physical process. With respect to the complexity and possible chaotic behaviors, the fundamental parameters are the minimum number of nonlinear equations associated with a physical mechanism, the embedding dimension, d_E, necessary to obtain an asymptotic value of the correlation dimension μ and the Kolmogorov entropy, κ, which is a measure of the loss of memory of the physical mechanism along the process. The mathematical process of the reconstruction theorem is based on the generation of m-dimensional space vectors,

$$Z(i) = \{x(i), x(i+1), \ldots, x(i+m--1)\}; \quad i = 1, \ldots, N, \qquad (2)$$

with$\{x(k)\}$ being the set of n elements of a empiric data series and $N = n - m + 1$. In terms of $Z(i)$, the correlation integral, following the Grassberger–Procaccia formulation (Grassberger and Procaccia, 1983a; 1983b), is written as

$$C(m, r) = \lim_{N\to\infty} \frac{1}{N^2} \sum\nolimits_{i,j=1}^{N} H\{r - \|Z(i) - Z(j)\ \|\}, \qquad (3)$$

with r being an Euclidean distance in the m-dimensional space and $H\{\cdot\}$, the Heaviside function. Equation (3) is the starting point to obtain numeric estimations of parameters μ and κ. Assuming that the correlation integral can be expressed as $C(m,r) = A_m\ e^{-m\kappa}$ $r^{\mu(m)}$, with A_m being the correlation amplitude for the reconstruction dimension m and plotting this correlation integral in terms of r on log–log scales,

$$\log\{C(m, r)\} = \log(Am) - m\kappa + \mu(m)\log(r), \qquad (4)$$

whose slope $\mu(m)$ is straightforwardly obtained for every reconstruction dimension m by means of linear regression on log–log scales. As mentioned in other papers related to this concept of correlation dimension (Burgueño *et al.*, 2014), two factors which could lead to wrong estimations of $\mu(m)$ have to be carefully revised. On one hand, the phenomenon of lacunarity (Turcotte, 1997), many times detected for small values of r; on the other hand, the saturation of $C(m, r)$ for high values of r. These shortcomings concerning $\mu(m)$ can be easily solved by searching for the r interval for which $\log\{C(m,r)\}$ is strongly linear dependent on $\log(r)$ and, at the same time, the highest square regression coefficient is detected. In this way, the slope of the log–log linear dependence becomes a good estimation of $\mu(m)$.

After a right quantification of the correlation dimension for every reconstruction dimension m, it is relevant to observe that $\mu(m)$ will tend asymptotically to a value, μ^*, which is interpreted as the minimum number of non-linear equations describing the mechanism that governs empiric data $\{x\}$. In this way, μ^* becomes a first evaluation of the complexity of the analyzed time series. It is also relevant that a high maximum dimension m or, in other words, a necessary high embedding dimension d_E for achieving the asymptotic value of $\mu(m)$, is usually associated with a random behavior of the analyzed time series.

Together with the degree of complexity and a possible random component of the physical mechanism, the loss of memory of the physical system is another valuable parameter. This question is quantified by the Kolmogorov entropy exponent, κ, which can be estimated as follows. According to Eq. (4) and Lana *et al.* (2010), grouping $\log\{C(m, r)\} - \mu(m)\log(r)$, as $\alpha(m)$,

$$\alpha(m) = \log(A_m) - m\kappa. \qquad (5)$$

This last equation permits a fast and accurate estimation of κ by a least square regression of empiric $\alpha(m)$ in terms of m, provided that $\log(A_m)$ should be a constant. Empirical data confirm this behavior only with m tending to ∞, being then assumed that A_{m+1}/A_m tends to 1.0 for high reconstruction dimensions m. In other words, correlation amplitudes tend to be very similar for high reconstruction dimensions.

Another relevant application of the reconstruction theorem is the quantification of the predictive instability. After generating m-dimensional vectors according to Eq. (2), in agreement with Wiggins (2003), the Lyapunov exponents, λ_j ($j = 1,2,\ldots,m$), can be computed according to the algorithms proposed by Eckmann *et al.* (1986) and Stopp and Meier (1988). Assuming that the addition of all the m Lyapunov exponents is negative, the trajectory in the m-dimensional space is described by aperiodic orbits around a strange attractor defined by the Kaplan–Yorke dimension, DKY (Kaplan and Yorke, 1979). Quantitatively,

$$D_{KY} = c + \frac{1}{|\lambda_{c+1}|} \sum_{j=1}^{c} \lambda_j \,, \tag{6}$$

with c being the maximum number of positive and negative Lyapunov exponents in a decreasing order, and accomplishing $\lambda_1 + \lambda_2 + \cdots + \lambda_c \geq 0$.

B. Multifractal spectrum

The concept of multifractal spectrum offers a new viewpoint of non-linear systems' complexity. At the same time, stablishes the multifractal characteristics (central Hölder exponent, extreme Hölder exponents, spectral amplitude and spectral asymmetry), as well as a synthesis of the physical mechanism degree complexity by taking advantage of a combination of Hölder exponents.

1. MDFA algorithm

The multifractal detrended fluctuaction analysis (MDFA) represents a reliable way of characterization of multifractal nonstationary and stationary time series (Kantelhardt *et al.*, 2002), the main objective being quantification of the rescaled structure of the q-order moments of the analyzed series, which is a process inherent to a multifractal structure analysis. It is worth mentioning that the MDFA offers higher quality and simplicity in comparison with other algorithms with similar objectives (Feder, 1988; Muzy *et al.*, 1994) and it has been applied to very different scientific fields such as human health, biology or Earth sciences, among others.

The MDFA algorithm can be summarized as the following five steps:

- Computation of the time series profile obtaining residuals from the average of the whole series.
- Segmentation of the profile. N_s non-overlapping segments of the profile, with equal length s, are generated. With the aim of improving computational accuracy, this second step is usually repeated starting from both extremes of the profile. In this way, $2N_s$ segments are available.
- Computation of the local variance for each one of the $2N_s$ segments. A least-square polynomial fit is computed for every segment and the residual variance of this fitting process is quantified for every segment, the non-stationarity of the series being then removed. In agreement with Koscielny-Bunde *et al.* (2006), polynomial degrees varying from 2 to 5 could be convenient.
- Computation of the qth-order fluctuation function, $F(s)_q$. This function is defined by Eqs. (7a) and (7b),

$$F(s)_q = \left\{ \frac{1}{2N_s} \sum_{1}^{2N_s} [F^2(s,\nu)]^{q/2} \right\}^{1/q}; \quad q \neq 0; -\infty < q < +\infty, \tag{7a}$$

$$F(s)_0 = \left\{ \frac{1}{4N_s} \sum_{1}^{2N_s} \ln[F^2(s,\nu)] \right\}; \quad q = 0. \tag{7b}$$

$F^2(s,\ \nu)$ is the local variance for every one of the $2N_s$ segments and parameter q is chosen varying within the +15, −15 range. Steps 2–4 have to be repeated for several segment lengths s. In agreement with Kantelhardt *et al.* (2002) useful values of s would be in the $m+2 \leq s < N/4$ interval, where m is the selected order for polynomial fits of step 3.

- *The scaling behavior of $F(s)_q$*. By assuming the hypothesis that the analyzed series are long-range power-law correlated, log–log plots of $F(s)_q$ vs s for each value of q accomplish the power-law given by Eq. (8),

$$F(s)_q \approx s^{h(q)}, \tag{8}$$

with the exponent $h(q)$ depending on q. If the analyzed series is non-stationary or noisy (fractal Brownian signals, for example), the exponent $h(q=2)$ will be equal to $H+1$, with H being the above introduced Hurst exponent. Conversely, for the stationary time series, as daily extreme temperatures or monthly atmospheric circulation indices, the exponent $h(q=2)$ is exactly the Hurst exponent H. The exponent $h(q)$ is many times also cited as the generalized Hurst exponent.

Differences between monofractal and multifractal behaviors have to be considered. Monofractal structures do not contribute very relevantly to obtain more information about the structure of the mechanism governing the analyzed series. Nevertheless, details offered by multifractal structures are much more complete. In the first case, variances $F^2(s,\nu)$ are identical or very similar for all segments s and the generalized Hurst exponent is reduced to the Hurst exponent H. Conversely, for multifractal behavior, segments with large variance dominate the q-order fluctuation function for positive q. Thus, the generalized Hurst exponent, $h(q)$, describes the scaling behavior of the segments with large fluctuations. Alternatively, for negative values of q, small fluctuations govern the q-order fluctuation function and then $h(q)$ describes the scaling behavior of the segments with small fluctuations (Movahed and Hermanis, 2008).

2. Singularity spectrum

The singularity spectrum $f(\alpha)$ [Eq. (9a)] is closely related to the q-order fluctuation function, $F(s)_q$, in terms of the generalized Hurst exponent, $h(q)$, and the Legendre transform

$$f(\alpha) = q\{\alpha - h(q)\} + 1 \tag{9a}$$

being also related the Hölder exponent α to the generalized Hurst exponent by Eq. (9b),

$$\alpha = h(q) + q\frac{dh(q)}{dq}, \tag{9b}$$

where α is also identified as the singularity strength or the Hölder exponent and $f(\alpha)$ represents the fractal dimension of the different subset of the series. The multifractal scaling exponent, $\tau(q)$, is defined as

$$\tau(q) = qh(q) - 1 \tag{10}$$

and the Hölder exponent α, in agreement with Eqs. (9b) and (10),

$$\alpha(q) = d\tau/dq. \tag{11}$$

The singularity spectrum provides new viewpoints of the multifractal structure of a series, given that $f(\alpha)$ quantifies the fractal dimensions of subsets of the series associated with the same singularity strength α. Several relevant fractal parameters related to the singularity spectrum have to be considered. One of them is the critical (central) Hölder exponent α_o, which corresponds to the maximum of $f(\alpha)$. A small value of α_o implies that the "fine-structure" of the physical mechanism cannot be analyzed from empiric data. Conversely, a large value of α_o strongly suggests the recovering of the "fine-structure." It is worth mentioning that the Hurst exponent, $H = h(q = 2)$, and α_o show a clear linear relationship, confirmed, for instance, by Burgueño *et al.* (2014). The other two relevant parameters, spectral asymmetry and spectral width, are related to the mathematical structure of $f(\alpha)$. The shape of this function is expected well fitted to a quadratic function [Eq. (12)] around the position α_o,

$$f(\alpha) = A(\alpha - \alpha_0)^2 + B(\alpha - \alpha_0) + C, \tag{12}$$

where C is an additive constant theoretically equal to 1, given that $f(\alpha)$ is defined as a normalized function with a maximum equal to 1.0, and B quantifies the asymmetry of the spectrum: $B = 0$ for a symmetric spectrum; $B > 0$ ("fine-structure") for a right-skewed spectrum; $B < 0$ ("smooth-structure") for a left-skewed spectrum. The spectrum width, W, defined as the range of α is defined as $W = \alpha_{\max} - \alpha_{\min}$, with $f(\alpha_{\max}) = f(\alpha_{\min}) = 0$. Bearing in mind that $\alpha_{\max}$ and $\alpha_{\min}$ are theoretically obtained by tending q to $\pm\infty$, these extreme Hölder exponents are estimated by extrapolating the fitted curve of Eq. (12) to zero. In short, the wider the range of the Hölder exponent, the stronger is the multifractality. Similarly, the wider the range of α, the "richer" is the structure of the physical process. As a summary, a series with a high value of α_0, a wide range of fractal exponents and a right-skewed shape is more complex than one with the opposite characteristics (Shimizu *et al.*, 2002). In terms of physical mechanism, a fine-structure could be analyzed provided that parameters α_o, B, and W confirm high complexity. On the contrary, only a smooth-structure of the physical mechanism would be obtained if the values of these three parameters suggest low complexity.

The complexity of the monthly rainfall multifractal structure can be summarized by the complexity index, CI, proposed by Shimizu *et al.* (2002). This global coefficient of complexity is defined by the addition of three normalized multifractal parameters, the central Hölder exponent, α_0, the multifractal amplitude, $(\alpha_{\max} - \alpha_{\min})$, and a new quantification of the asymmetry $(\alpha_{\max} - \alpha_0)/(\alpha_0 - \alpha_{\min})$. In agreement with this definition of the asymmetry, a quotient very close (or equal) to 1.0 will imply high (absolute) symmetry. Conversely, a left asymmetry will be characterized by a quotient lower than 1.0 and a right asymmetry by a quotient higher than 1.0. The asymmetry could be also directly represented by the coefficient B of Eq. (12). Nevertheless, this coefficient could be sometimes affected by computational uncertainties due to a relative bad fit of empirical data to the mentioned Eq. (12).

In short, whereas high positive values of CI would imply a notable complexity on the physical mechanisms governing the analyzed phenomena, negative and lower positive CI's would be associated with more simple physical mechanisms. In consequence, high positive values of CI would be associated with difficult success predictability. Conversely, negative or low positive values of CI would suggest an easier predictability.

Finally, it is straightforward to conclude that the monofractality will be characterized by a singularity spectrum $f(\alpha) = 1.0$ of null width. This fact would imply that the dependence of $h(q)$ on q disappears, and it is reduced to the Hurst exponent H, which at the same time is coincident with the single Hölder exponent α. In short, it is evident that a monofractal structure has to be assumed notably less complex than a multifractal structure.

TABLE I. Minimum, maximum, mean, standard deviation, SD, and skewness, Sk, of the RFT parameters for the 96 records.

	Min	Max	Mean	SD	Sk
H	0.37	0.70	0.55	0.06	0.338
λ_1	0.11	0.22	0.16	0.02	0.316
D_{KY}	11.99	13.62	12.66	0.38	0.286
μ^*	6.71	9.75	8.18	0.60	0.205
K	0.54	2.31	1.64	0.31	−0.643

IV. RESULTS

A relatively complex spatial distribution of the fractal parameters has to be expected due to, as mentioned in Sec. II, the complex orography including several mountain chains, a central basin, and proximity to the Mediterranean coast. As a consequence, a revision of several characteristics concerning RFT and MDFA parameters is necessary to detect places where the physical processes governing the monthly rainfall would be relatively easy or complex. First of

TABLE II. Cross-correlation coefficients between different pairs of FRT parameters. Bold types correspond to coefficients very close to 1.0 and exceeding 95% statistical confidence.

H	λ_1	−0.10
$\boldsymbol{H}$	$\boldsymbol{D_{KY}}$	−0.19
$\boldsymbol{H}$	$\boldsymbol{\mu^*}$	0.03
$\boldsymbol{H}$	$\boldsymbol{K}$	−0.03
$\boldsymbol{\lambda_1}$	$\boldsymbol{D_{KY}}$	**0.86**
$\boldsymbol{\lambda_1}$	$\boldsymbol{\mu^*}$	**0.89**
$\boldsymbol{\lambda_1}$	$\boldsymbol{K}$	0.05
$\boldsymbol{D_{KY}}$	$\boldsymbol{\mu^*}$	−0.53
$\boldsymbol{D_{KY}}$	$\boldsymbol{K}$	0.13
$\boldsymbol{\mu^*}$	$\boldsymbol{K}$	0.29

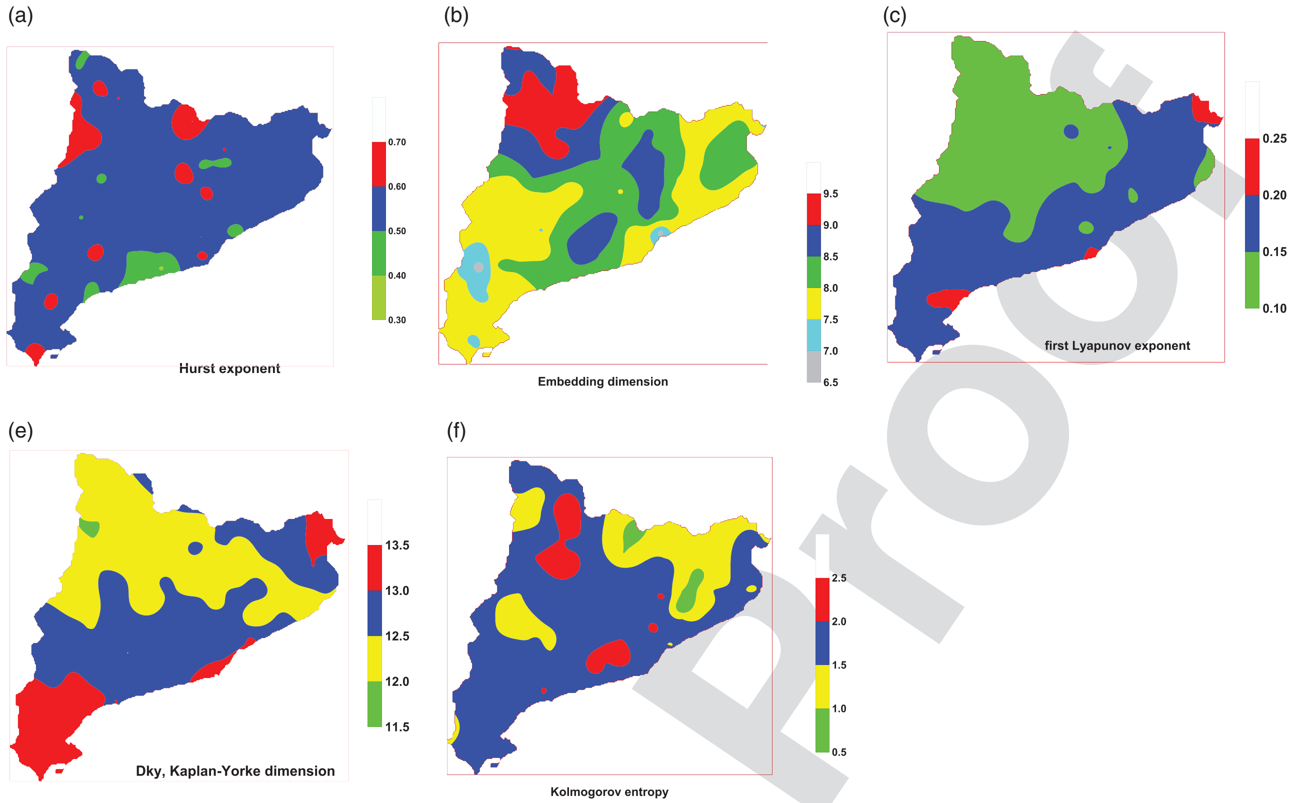

FIG. 4. Spatial distribution of (a) Hurst exponents, (b) embedding dimensions, (c) first Lyapunov exponents, (d) Kaplan–Yorke dimension, and (e) Kolmogorov entropy.

all, the predominant and extreme parameter values are introduced and their meaning, with respect to the complexity of the physical mechanism, are discussed. After that, more details are given with respect to the spatial distribution of these parameters and possible relationships to orography and proximity to the Mediterranean Sea.

A. Reconstruction fractal theorem

(a) *The Hurst exponent*: With respect to parameters obtained from the RFT (Table I), the Hurst exponent is characterized by predominant values slightly exceeding 0.5 (showing signs of persistence), manifested by a skewness of 0.34, average and standard deviation of 0.55 and 0.06, respectively, and only a few cases with low and high Hurst exponents, implying anti-persistence and persistence, respectively. The spatial distribution of this exponent (Fig. 4) is characterized by a domain of quasi-randomness behavior (H varying from 0.4 to 0.6) covering almost all the analyzed area, and some isolated emplacement of clear anti-persistence ($H < 0.4$) and persistence ($H > 0.6$). In short, the monthly rainfall regime could be assumed with a few notable signs of persistence and anti-persistence and predominant behavior close to randomness. This predominance would be an impediment on autoregressive processes leading to compute forthcoming monthly amounts.

(b) *The embedding dimension*: The minimum number of necessary non-linear equations, represented by μ^*, to quantify the monthly rainfall series is characterized by a relatively long interval (6.71–9.75), with average and standard deviations of 8.18 and 0.60, respectively, and a low skewness (Table I). A high ratio of embedding dimensions is within the interval (7.25–9.0). Consequently, due to these high values of μ^*, the autoregressive process to quantify forthcoming monthly amounts is expected to be complex. The spatial distribution of μ^* (Fig. 4) detects the Central Basin and some isolated emplacement of the Mediterranean coast with relatively low values of μ^*. It is also relevant signs of an increasing tendency toward the North-eastern and, especially, toward the North-western (Pyrenees domain). In short, the monthly rainfall regime would be characterized by more complex mechanisms (systems of non-linear equations), especially in these two just mentioned areas.

(c) *The predictive instability*: The instability, in other words, the uncertainty on forthcoming predicted monthly amounts, is notably governed by the first Lyapunov exponent. Its values are delimited by a short range from 0.11 to 0.22, with a very small standard deviation (0.02) and a notable number of samples exceeding an average of 0.16 (Table I). A high ratio of monthly rainfall amounts are characterized by λ_1 varying from 0.125 to 0.175. In agreement with Fig. 4, besides two small areas at the

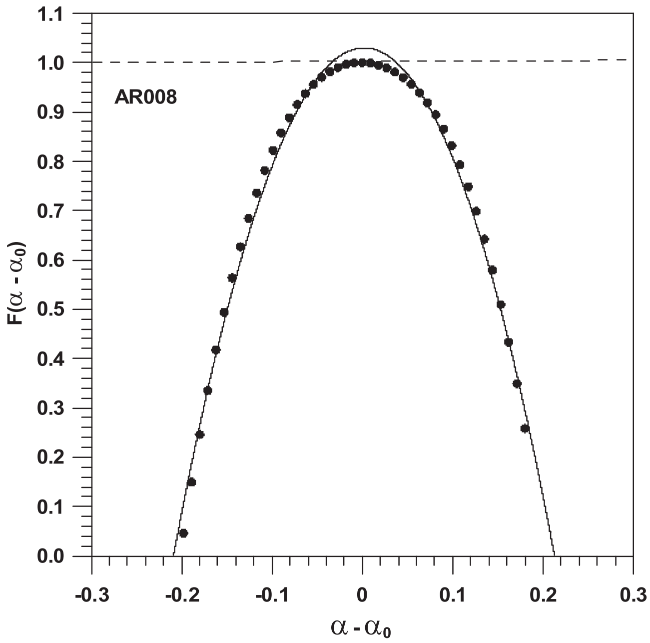

FIG. 5. An example of multifractal spectrum corresponding to a gauge in North-Western Catalonia. Solid points represent empirical samples of multifractality for a wide range of α(q) parameters. The continuous line describes the theoretical multifractal spectrum, given by a second order polynomial.

North-east and the South-west with the highest values, this first Lyapunov exponent is characterized by two well defined areas; one of them approximately covering the Mediterranean coast, Littoral, and Pre-littoral chains and the beginning of the Eastern Pyrenees; the other corresponding to the rest of the analyzed domain, including a good part of the North-western Catalonia and most of the Eastern Pyrenees chain.

(d) *Kaplan–Yorke dimension*: The Kaplan–Yorke dimension is characterized by a narrow range (11.99–13.62), an average of 12.66, a moderate standard deviation (0.38), and skewness (0.29) (Table I), and a high ratio of monthly series with D_{KY} ranging from 12.25 to 13.25. Due to its expected relation to the Lyapunov exponents (specially the first exponent), a spatial structure, similar to that observed for λ_1, should be expected, excepting for the range of (12.0–12.5) of Kaplan–Yorke dimensions expanding along a narrow fringe up to the Northern Mediterranean coast (Fig. 4). In short, higher predictive instabilities have to be expected toward the South and North-east of the Catalonia.

(e) *The loss of memory of the physical system*: The measure of the loss of memory of the physical system (the Kolmogorov exponent *K*), is characterized by a wide range (0.54–2.31) and standard deviations and average values of 0.31 and 1.64 (Table I). Nevertheless, a high number of cases are within the (1.5–2.0) interval. Consequently, most of the monthly rainfall patterns would be characterized by outstanding loss of memory. Then, the necessary number of monthly amounts to obtain a reliable estimation of the next amount would be high, this fact making complex an autoregressive process. The spatial distribution of *K* is not very homogeneous (Fig. 4) and distinction has to be made between a clear dominant area with *K* ranging from 1.5 to 2.5 and another lowering 1.5. In consequence, two regions are detected. On one hand, an area representing a high ratio of the domain where the loss of memory is relevant; on the other hand, a more reduced area (North-eastern and some Western emplacements), where the loss of memory of the physical system is notably smaller.

TABLE III. Minimum, maximum, mean, standard deviation, SD, and skewness, Sk, of the MDFA parameters.

	Min	Max	Mean	SD	Sk
α_0	0.36	0.66	0.50	0.05	0.101
α_{max}	0.55	0.91	0.72	0.07	0.184
α_{min}	0.02	0.55	0.27	0.09	−1.471
W	0.18	1.01	0.44	0.12	1.530
Γ	−4.45	2.50	−0.05	1.18	−0.404
CI	−2.83	2.52	0.00	1.00	−0.071

Table II also summarizes possible relationships among the different RFT parameters. The notable cross-correlation between the first Lyapunov exponent and the Kaplan–Yorke Yorke dimension could be expected bearing in mind Eq. (6), where the dependence of D_{KY} on the Lyapunov exponents is quite evident. Beside this first high cross-correlation, it is also very relevant the correlation between the first Lyapunov exponent, λ_1, and the dimension μ^*. In agreement with the meaning of these two fractal parameters, the predictive instability would increase with the number of nonlinear equations describing the physical mechanism of the successive monthly rainfall amounts.

B. Multifractal detrended fluctuation analysis

An example of multifractal spectrum is shown in Fig. 5. This spectrum has been obtained from monthly rainfall records belonging to a raingauge emplaced in the Pyrenees. Solid points are the empiric samples of multifractal spectrum for a wide range of q exponents, within the $\pm\infty$ interval. The solid line is the quadratic polynomial given by Eq. (12), and the dashed horizontal line delimits the maximum expected multifractal amplitude $f(\alpha{-}\alpha_0) = 1.0$. In spite of the good fit of empiric multifractallity to Eq. (12), the theoretical maximum is slightly higher than 1.0, which is a, sometimes detected, not very relevant shortcoming. The example of this figure is also a good example of almost null asymmetry ($\gamma \approx 0$), given that the extrapolated values to determine the extremes ($\alpha_{max} - \alpha_0$) and ($\alpha_{min} - \alpha_0$) are very close to ± 0.21, leading to a spectral amplitude close to 0.42. In agreement with Table III, these last two values are very close to the average of W and γ when the whole sample of 96 parameters is analyzed.

(a) *The central α_0 Hölder exponent*: This multifractal parameter, characterizing the complexity of the physical process, is identified by extreme values of 0.36 (low complexity) and 0.66 (high complexity). Bearing in mind that its average and standard

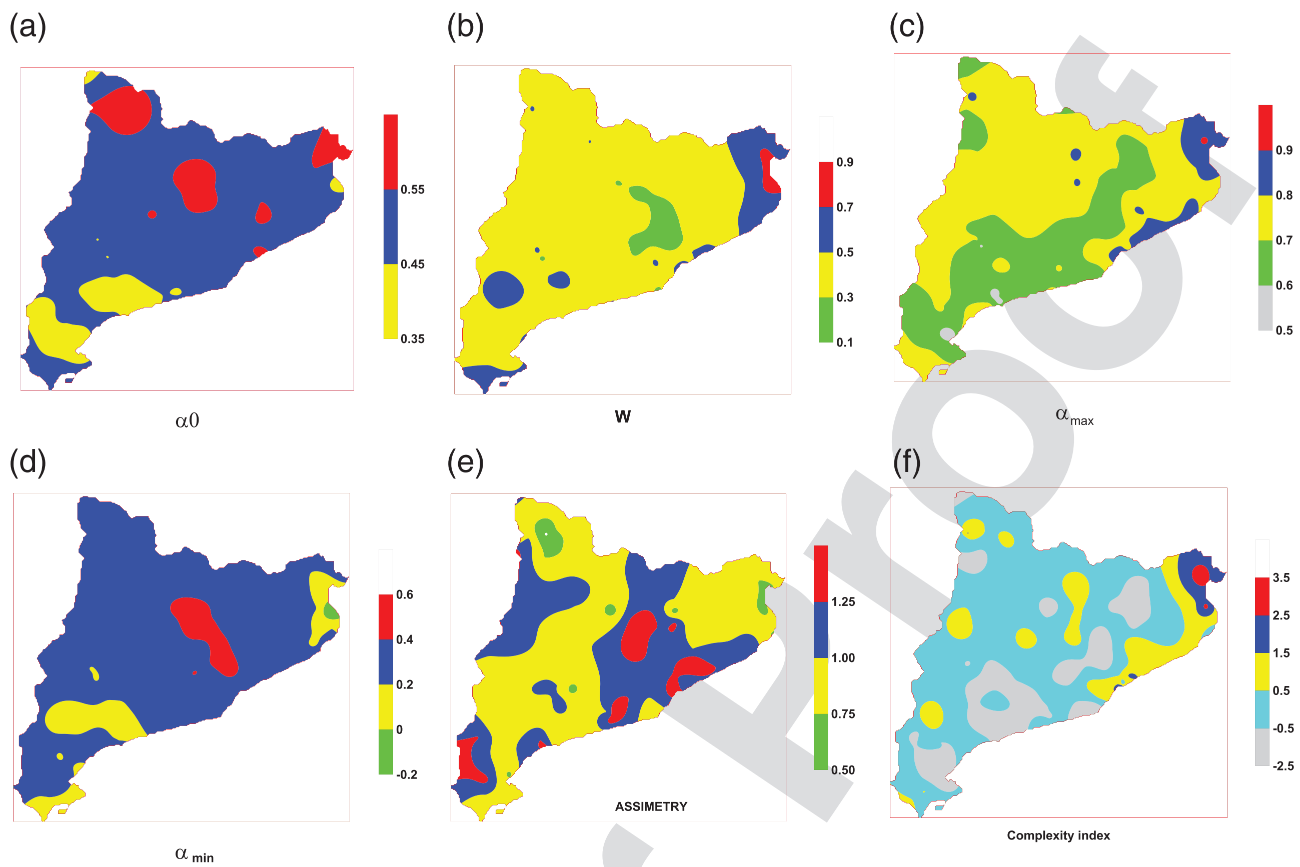

FIG. 6. Spatial distribution of (a) the central Hölder exponent, (b) spectral amplitude, (c) maximum and (d) minimum Hölder exponents, (e) spectral asymmetry, and (f) complexity index.

deviation are 0.50 and 0.05, respectively, and the low skewness (0.101) (Table III), most of the α_0 values are detected within the interval (0.35–0.45) which would represent physical processes of moderate complexity. Nevertheless, bearing in mind the contribution of the other two parameters, multifractal spectral amplitude W and asymmetry γ, the degree of physical complexity will be finally quantified by means of the index CI. With respect to the spatial distribution of the central Hölder exponent (Fig. 6), it is evident that a great part of Catalonia is characterized by α_0 within the 0.45–0.55 interval. Only toward the south, for some areas, α_0 is less than 0.45 (minor complexity). Opposite to this, for some places on the North, not necessarily emplaced in the Pyrenees, the parameter exceeds 0.55, describing higher complexity. At least for this multifractal parameter, the proximity to the Mediterranean coast and the Pyrenees, or the emplacement on the Central Basin, are factors not conditioning α_0.

(b) *The maximum, α_{max}, and minimum, α_{min}, Hölder exponents*: In agreement with Table III, $\alpha_{\max}$ and $\alpha_{\min}$ are characterized by small standard deviations (0.09 and 0.05, respectively) and a moderate skewness on $\alpha_{\max}$. Most of the values of these parameters are detected within narrow ranges (0.65–0.80 for $\alpha_{\max}$ and 0.20–0.35 for $\alpha_{\min}$). From the spatial point of view (Fig. 6), $\alpha_{\max}$ with values from 0.7 to 0.8 covers a great area, being also notable the domain characterized by values within the 0.6–0.7 interval. Are also outstanding some small isolated domains along the Mediterranean coast where $\alpha_{\max}$ exceeds 0.8. $\alpha_{\min}$ varying from 0.2 to 0.4 covers a great portion of the map, being also worthy of mention two small nuclei (0.0–0.2 and 0.4–0.6). Although both extreme Hölder parameters contribute to the quantification of the complexity, emplacements with similar behaviors on $\alpha_{\max}$ and $\alpha_{\min}$ are difficult to detect. For this reason, for a better characterization of the complexity, the spectral amplitude W can be considered, ranging from 0.18 to 1.01, an average and standard deviation of 0.44 and 0.12, a very relevant skewness of 1.53 (Table III), and with many of the W samples within the (0.30–0.55) interval. Bearing in mind the notable value of the skewness, a quite heterogeneous spatial distribution of this last index could be expected. Nevertheless, Fig. 6 describes a great portion of Catalonia associated with spectral amplitudes from 0.3 to 0.5, being also detected the widest amplitudes on two reduced domains of the Mediterranean coast

TABLE IV. Cross-correlation, CCor, for pairs of MDFA parameters. Bold types correspond to coefficients exceeding 95% statistical confidence level.

Pairs of MDFA	CCor
α_0, α_{max}	**0.60**
α_0, W	−0.12
α_0, γ	−0.04
α_0, CI	0.52
α_{max}, W	**0.64**
α_{max}, γ	0.07
α_{max}, CI	**0.89**
W, γ	−0.24
W, CI	0.48
γ, CI	0.42

(North-east and South-west extremes) and the narrowest ones on a small area in the Pre-Littoral chain.

(c) *The asymmetry*: Another point of view of the complexity is offered by the asymmetry γ, with extreme values varying from −4.45 (strong left asymmetry) to 2.50 (strong right asymmetry). The average of all the 96 asymmetry samples is almost null (−0.05) and the standard deviation is 1.18 (Table III). In agreement with Fig. 6, the most common range of asymmetry is from 0.75 to 1.0 and from 1.0 to 1.25. Both positive ranges would be associated with right asymmetries of the multifractal spectra, characterizing signs of complexity. Exceptionally, the highest right asymmetries (γ exceeding 1.25) are detected in reduced areas on the Central Basin, the Mediterranean coast, and the inner Catalonia. Conversely, the left asymmetries (γ lowering 0.75 appear in reduced areas and, especially, on the north face of the Eastern Pyrenes).

(d) *The complexity index*: Taking into account the possibility of monthly rainfall series associated with very different values of α_0, W, and γ, the index CI is finally chosen as the best parameter to define the complexity of every monthly rainfall series. This index is characterized (Table III) by extremes of −2.83 (low complexity) and 2.52 (high complexity), with moderate symmetry (skewness equal to 0.071) and a clear predominance of monthly series, 71 out of 96 cases, within the (−1.0, +1.0) interval. The spatial distribution of CI can be described (Fig. 6) by a few places with low values (<-0.5), being an example the mouth of the Ebro river and neighboring domains, at the southern extreme, prevalence of a very moderate complexity (−0.5, 0.5) throughout the country and outstanding values of CI (strong complexity) toward the North-eastern extreme.

Possible correlations among the different multifractal parameters are summarized in Table IV. The cross-correlation coefficients certainty has been quantified, in agreement with Hirsch *et al.* (1992), being obtained in all cases cross-correlations exceeding 90%–95% significant levels. It is noticeable the strong positive correlation between α_{max} and CI as well as the notable correlations between α_{max} and W and α_{max} and α_0. It is also worth mentioning that the weight of the central Hölder exponent α_0, the multifractal spectral amplitude W, and the asymmetry γ on the parameter CI is quite similar by revising the corresponding cross-correlation coefficients. Consequently, besides the strong correlation between α_{max} and CI, the complexity of the physical mechanism governing the monthly rainfall regime is due to a similar weighted contribution of the central Hölder exponent, the multifractal spectral amplitude, and asymmetry.

V. CONCLUSIONS

The analysis of the fractal/multifractal structure of the monthly rainfall regime in Catalonia permits to confirm from a new viewpoint the heterogeneous spatial distribution of monthly rainfall patterns. This heterogeneous distribution, in spite of a relatively reduced geographic domain, would be the consequence of a complex orography, with a notable range of altitudes from zero meters above sea level (Mediterranean coast) up to 3000 m (Pyrenees) and the different mountain chains (Eastern Pyrenees, Littoral, and Pre-Littoral chains) and a wide Central Basin. Bearing in mind the predominant NW frontal passages form the Atlantic Ocean and the Eastern advections on the Mediterranean Sea, these one especially in autumn, the effects of the topographic barriers created by the mountain chains on local rainfall regimes are expected. Additionally, the proximity or remoteness to the Mediterranean coast is another factor to be considered.

Concepts as randomness/persistence, uncertainties on forecasting processes, the complexity degree of the non-linear equations describing the physical process, its loss of memory, and a combined set of multifractal parameters, leading to quantifying the complexity of the monthly rainfall regime, have permitted to accomplish two relevant objectives. First, a new and complete classification of rainfall pattern areas, bearing in mind the spatial distribution of the different fractal/multifractal parameters describing properties of the rainfall regime. Second, the detection of rainfall regimes needing a high, low, or moderate number of consecutive monthly amounts previous to the forthcoming amount obtained by autoregressive processes. Additionally, places where the uncertainty and the discrepancy between forecasted and really recorded amounts would be high, low, or moderate are also detected. These results, concerning number of necessary monthly amounts and discrepancies between real and forecasted amounts, are relevant bearing in mind that the analyzed Mediterranean region is characterized by long dry spells. Then, accurate autoregressive processes are necessary to forecast forthcoming monthly amounts preventing or mitigating the effects of these long dry spells. Consequently, the next step on the increasing knowledge about the monthly rainfall regime in Catalonia should be the application of autoregressive processes, bearing in mind results obtained in this paper from the viewpoint of the fractal/multifractal theory. Additionally, validation of possible time trends on monthly amounts should be also considered.

DATA AVAILABILITY

The monthly scale data that support the findings of this research are available from the corresponding author upon reasonable requests. Daily scale data are also available from the meteorological agency of Catalonia (SMC, www.meteo.cat), Ref. ■; Fabra Observatory *(Reial Acadèmia de Ciències i Arts, RACA*, Barcelona);

and Ebre Observatory (*Ramon Llull University*, ■, *and Consejo Superior de Investigaciones Científicas*, Spanish Government).

REFERENCES

Burgueño, A., Lana, X., Serra, C., and Martínez, M. D., "Daily extreme temperature multifractals in Catalonia (NE Spain)," Phys. Lett. A **378**, 874–885 (2014).

Casas-Castillo, M. C., Llabrés-Brustenga, A., Rius, A., Rodríguez-Solà, R., and Navarro, X., "A single scaling parameter as a first approximation to describe the rainfall pattern of a place: Application on Catalonia," Acta Geophys. **66**, 415–424 (2018).

Clavero, P., Martín-Vide, J., and Raso, J., "*Atles climàtic de catalunya: Termopluviometria*" (Departament de Medi Ambient, Generalitat de Catalunya, 1996), pp. 1–42.

Diks, C., "Nonlinear time series analysis. Methods and applications," in *Nonlinear Time Series and Chaos*, edited by H. Tong (World Scientific, London, 1999), Vol. 4, p. 209.

Dimri, V. P., "Fractals in geophysics and seismology: An introduction," in *Fractal Behaviour of the Earth System* (Springer, Berlin, 2005), pp. 1–22.

Eckmann, J. P., Oliffson, S., Ruelle, D., and Cilliberto, S., "Lyapunov exponents from time series," Phys. Rev. A **34**, 4971–4979 (1986).

Enescu, B., Ito, K., Radulian, M., Popescu, E., and Bazacliu, O., "Multifractal and chaotic analysis of Vrancea (Romania). Intermediate-depth earthquakes: Investigation of the temporal distribution of events," Pure Appl. Geophys. **162**, 249–271 (2005).

Feder, J., *Fractals* (Plenum Press, New York, 1988), p. 147.

García-Marín, A., Estévez, J., Alcalá-Miras, J. A., Morbidelli, R., Flammini, A., and Ayuso-Muñoz, J. L., "Multifractal analysis to study break points in temperature data sets," Chaos **29**, 093116 (2019).

García-Marín, A., Estévez, J., Jiménez-Hornero, F. J., and Ayuso-Muñoz, J. L., "Multifractal analysis of validated wind speed time series," Chaos **23**, 013133 (2013).

Godano, C., Alonzo, M. L., and Bottari, A., "Multifractal analysis of the spatial distribution of earthquakes in southern Italy," Geophys. J. Int. **125**, 901–911 (1996).

Goltz, C., "Fractal and chaotic properties of earthquakes," in *Lecture Notes in Earth Sciences* (Springer, Berlin, 1997), Vol. 77, p. 178.

Grassberger, P. and Procaccia, I., "Characterization of strange attractors," Phys. Rev. Lett. **50**, 346–349 (1983a).

Grassberger, P. and Procaccia, I., "Estimation of the Kolmogorov entropy from a chaotic signal," Phys. Rev. A **28**, 448–451 (1983b).

Herrera-Grimaldi, P., García-Marín, A., and Estévez, J., "Multifractal analysis of diurnal temperature range over southern Spain using validated datasets," Chaos **29**, 063105 (2019).

Hirabayashi, T., Ito, K., and Yoshii, T., "Multifractal analysis of earthquakes," in *Fractals and Chaos in the Earth Sciences* (Springer, 1992), pp. 591–610.

Hirsch, R. M., Helsel, D. R., Cohn, T. A., and Gilroy, E. J., "Statistical analysis of hydrologic data," in *Handbook of Hydrology*, edited by D. R. Maidment (McGraw-Hill, New York, 1992), pp. 17.1–17.55.

Kantelhardt, J. W., Zschiegner, S. A., Koscielny-Bunde, A., Havlin, S., Bunde, A., and Stanley, H. E., "Multifractal detrended fluctuation analysis of nonstationary time series," Phys. A Stat. Mech. Appl. **316**, 87–114 (2002).

Kaplan, J. K. and Yorke, J. A., "Chaotic behaviour of multidimensional difference equations," in *Functional Difference Equations and Approximation of Fixed Points*, edited by H. O. Walter and H. O. Peitgen (Springer, Berlin, 1979), Vol. 730, pp. 204–227.

Korvin, G., *Fractal Models in the Earth Sciences* (Elsevier, Amsterdam, 1992), p. 396.

Koscielny-Bunde, E., Bunde, S., Havlin, S., Roman, H. E., Goldreich, Y., and Schellnhuber, H. J., "Indication of a universal persistence law governing atmospheric variability," Phys. Rev. Lett. **81**, 729–732 (1998).

Koscielny-Bunde, E., Kantelhardt, J. W., Braund, P., Bunde, A., and Havlin, S., "Long-term persistence and multifractality of river runoff records: Detrended fluctuation studies," J. Hydrol. **322**, 120–137 (2006).

Lana, X., Burgueño, A., Martínez, M. D., and Serra, C., "Complexity and predictability of the monthly western Mediterranean oscillation index," Int. J. Climatol. **36**, 2435–2450 (2016).

Lana, X., Burgueño, A., Serra, C., and Martínez, M. D., "Fractal structure and predictive strategy of the daily extreme temperature residual at fabra observatory (NE Spain, years 1917-2005)," Theor. Appl. Climatol. **121**, 225–241 (2015).

Lana, X., Burgueño, A., Serra, C., and Martínez, M. D., "Monthly rain amounts at fabra observatory (Barcelona, NE Spain): Fractal structure, autoregressive processes and correlation with monthly western Mediterranean oscillation index," Int. J. Climatol. **37**, 1557–1577 (2017).

Lana, X., Martinez, M. D., Serra, C., and Burgueno, A., "Complex behaviour and predictability of the European dry spell regimes," Nonlinear Processes Geophys. **17**, 499–512 (2010).

Llabrés-Brustenga, A., Rius, A., Rodríguez-Solà, R., Casas-Castillo, M. C., and Redaño, A., "Quality control process of the daily rainfall series available in catalonia from 1855 to the present," Theor. Appl. Climatol. **137**, 2715–2729 (2019).

Mandelbrot, B. B., *The Fractal Geometry of Nature*(WH Freeman and Co., New York, 1983), revised and enlarged edition, p. 495.

Mc Night, T. L. and Hess, D., "Climate zone and types," in *Physical Geography. A Landscape Appreciation* (Prentice Hall, Upper Saddle River, NJ, 2000), p. 200.

Movahed, M. S. and Hermanis, E., "Fractal analysis of river flow fluctuations," Phys. A **387**, 915–932 (2008).

Muzy, J. F., Bacry, E., and Arneodo, A., "The multifractal formalism revisited with wavelets," Int. J. Bifurc. Chaos **4**, 245–302 (1994).

Ozturk, S., "Statistical correlation between b-value and fractal dimension regarding Turkish epicenter distribution," Earth Sci. Res. J. **16**(2), 103–108 (2012).

Press, W. H., Teukolsky, S. A., Vetterling, W. T., and Flannery, B. P., "Interpolation by kriging," in *Numerical Recipes: The Art of Scientific Computing*, 3rd ed. (Cambridge University Press, New York, 2007), Sec. *3.7.4*.

Rodríguez, R., Casas, M. C., and Redaño, A., "Multifractal analysis of the rainfall time distribution on the metropolitan area of Barcelona (Spain)," Meteorol. Atmos. Phys. **121**, 181–187 (2013).

Shimizu, Y., Thurner, S., and Ehrenberger, K., "Multifractal spectra as a measure of complexity human posture," Fractals **10**, 104–116 (2002).

Stein, M. L., *Statistical Interpolation of Spatial Data: Some Theory for Kriging* (Springer, New York, 1999).

Stoop, F. and Meier, P. F., "Evaluation of Lyapunov exponents and scaling functions from time series," J. Opt. Soc. Am. B **5**, 1037–1045 (1998).

Talkner, P. and Weber, R. O., "Power spectrum and detrended fluctuation analysis: Application to daily temperatures," Phys. Rev. E **62**(1), 150–160 (2000).

Turcotte, D. L., *Fractal and Chaos in Geology and Geophysics*, 2nd ed. (Cambridge University Press, Cambridge, 1997), p. 398.

Wiggins, S., "Introduction to applied nonlinear dynamical systems and chaos," in *Texts in Applied Mathematics*, 2nd ed. (Springer, New York, 2003), Vol. 2, p. 844.